MATERIALS CHEMISTRY FRONTIERS

RESEARCH ARTICLE

View Article Online
View Journal | View Issue

Cite this: *Mater. Chem. Front.*, 2025, **9**, 3026

Solvent-induced crystal engineering for enhanced room-temperature phosphorescence in copper(I) iodide clusters

Yan-Ting Huang,[a] Wen He,[a] Jun-Zhe Dong,[a] Ya-Nan Fan,[a] Zhang-Wen Wei [a] and Mei Pan *[ab]

Received 26th August 2025,
Accepted 2nd September 2025

DOI: 10.1039/d5qm00636h

rsc.li/frontiers-materials

Based on crystalline polymorphism, we utilized a solvent-mediated crystal engineering strategy to synthesize three polymorphic copper-iodide clusters, **1** [Cu_4I_4(4-dpda)$_4$], **1-Tol** [Cu_4I_4(4-dpda)$_4$·C_7H_8], and **1-PX** [Cu_4I_4(4-dpda)$_4$·C_8H_{10}] (4-dpda = 4-(diphenylphosphino)-*N*,*N*-dimethylaniline), respectively. The polymorphic clusters not only exhibit significant differences in their crystal structures but also manifest remarkable changes in their room-temperature phosphorescence (RTP), high energy (HE)/low energy (LE) energy transfer barriers, and thermal quenching properties. Through comprehensive analysis of the single crystal structure, spectroscopic measurements and theoretical calculation, we elucidated the distinct mechanisms by which solvent-mediated crystal engineering enhances RTP performance. Furthermore, based on the significantly enhanced thermochromic effect, the potential of **1-Tol** as a luminescent thermometer with dual-temperature-zone response characteristics was explored, achieving a notable improvement in sensitivity in the low-temperature region. In contrast, **1-PX** broadened the response range of thermochromic sensing.

Introduction

Luminescent materials exhibiting room temperature phosphorescence (RTP) have attracted increasing attention due to their fundamental importance and broad application prospects.[1–4] For OLED applications, RTP materials can achieve 100% internal quantum efficiency because they can harvest both singlet and triplet excitons, a value much higher than that of fluorescent materials, which only emit through singlet excitons and therefore can only reach a theoretical efficiency four times lower.[5,6] The large Stokes shift and long lifetime emission of phosphorescence offer significant advantages in applications such as sensing, bioimaging, light-emitting diodes, and anti-counterfeiting technologies.[7–11]

Copper(I) iodide clusters have gained significant attention as luminescent materials due to their low cost, environmental friendliness, and diverse coordination structures,[12–14] overcoming the high cost and scarcity issues associated with noble metal complexes such as iridium and platinum.[15] More importantly, the d^{10} electronic configuration of copper(I) effectively prevents the d-d excited state, significantly reducing non-radiative deactivation pathways, thereby laying the foundation for their applications in high-efficiency RTP materials.[16] Copper(I) iodide clusters exhibit a variety of energy transfer modes, such as cluster-centered (CC) emission, metal-to-ligand charge transfer (MLCT), and halogen-to-ligand charge transfer (XLCT).[17] At room temperature, the luminescence is mainly dominated by cluster-centered emission bands with longer wavelength, while at low temperature, these bands become weak, and the luminescence is mainly dominated by high-energy XLCT emission bands with shorter wavelength, resulting in the typical thermochromic phenomenon. However, the subtle energy level differences among multiple triplet states induce vibrational coupling and their subsequent merging into one of the triplet states, leading to non-radiative deactivation and thereby suppressing RTP.[18] Meanwhile, a critical challenge lies in the so-called thermal quenching (TQ) effect of luminescence, which refers to the significant loss of luminescence intensity as the temperature increases due to accelerated non-radiative decay processes competing with radiative transitions.[19,20]

To enhance the RTP efficiency of copper(I) iodide clusters, a variety of strategies have been developed, including ligand engineering,[21–24] aggregation-induced emission (AIE),[25,26] crystal engineering,[27–29] and guest-induced phosphorescence.[30,31] However, the fundamental mechanism for enhancing RTP performance remains poorly understood to date. It is well

[a] *MOE Laboratory of Bioinorganic and Synthetic Chemistry, Lehn Institute of Functional Materials, IGCME, GBRCE for Functional Molecular Engineering, School of Chemistry, Sun Yat-Sen University, Guangzhou 510006, China*
[b] *College of Chemistry, Xinjiang University, Urumqi 830046, China. E-mail: panm@mail.sysu.edu.cn*

recognized that precise crystal structure determination is key to unraveling the structure–property relationships at the molecular level, while crystal engineering provides a systematic approach to optimize these relationships. Polymorphic luminescent supramolecular systems are particularly significant in crystal engineering, as they often exhibit diverse photoluminescent characteristics.[32–34] Systematic investigations of these systems can reveal the direct correlation between molecular structures and optical properties, offering crucial guidance for designing highly efficient luminescent materials through crystal engineering. Furthermore, in the design and synthesis of metal clusters, solvent selection in crystal engineering plays a critical role.[35–37] Solvents not only participate in the self-assembly and crystallization processes of complexes but also significantly influence the molecular configurations and crystal forms of the products, directly impacting the efficiency and stability of RTP.

In this work, three polymorphic copper(I) iodide clusters, namely, **1** [Cu_4I_4(4-dpda)$_4$], **1-Tol** [Cu_4I_4(4-dpda)$_4$·C_7H_8], and **1-PX** [Cu_4I_4(4-dpda)$_4$·C_8H_{10}] (4-dpda = 4-(diphenylphosphino)-*N*,*N*-dimethylaniline) were successfully constructed through a crystal engineering strategy in acetonitrile, toluene, and *p*-xylene, respectively, exhibiting significant differences in their crystal structures. Notably, optimization ***via*** crystal engineering significantly enhanced the RTP intensities of **1-Tol** and **1-PX**, with their photoluminescence quantum yield (PLQY) reaching 12 times and 7 times that of **1**, respectively. Combined single-crystal structural analysis and spectroscopic studies revealed that the crystal engineering in **1-Tol** and **1-PX** modulates the emissive states of low energy (LE) and high energy (HE) emission, as well as their energy transfer, through distinct mechanisms. This effectively suppresses TQ and significantly enhances RTP. These differences not only reflect the regulatory role of solvents during crystal growth but also highlight the central importance of crystal engineering in the precise design and structural control of materials. Furthermore, based on the remarkable thermochromic effects achieved through crystal engineering, we further explored the application potential of **1-Tol** and **1-PX** in temperature-sensing response and multicolor display.

Results and discussion

As shown in Fig. 1a, three polymorphic cubane Cu_4I_4(4-dpda)$_4$ (4-dpda = 4-(diphenylphosphino)-*N*,*N*-dimethylaniline) based crystals (**1**, **1-Tol**, and **1-PX**) were successfully synthesized through the reaction of CuI and the ligand 4-dpda in different solvents (acetonitrile, toluene, and *p*-xylene). Among these, the crystal structure of **1** is the same as previously reported,[38] but here we mainly focus on its photophysical-structure relationship with **1-Tol**, and **1-PX**. PXRD results indicate that the obtained products possess high purity and excellent crystallinity (Fig. S1). X-ray crystallography (Tables S1–S3) reveals that the basic units of **1**, **1-Tol**, and **1-PX** are all composed of a distorted cubic Cu_4I_4 core and four 4-dpda ligands. Although **1** and **1-Tol** belong to the same space group ($P\bar{1}$), the presence of toluene solvent molecules in **1-Tol** leads to significant differences in their unit cell parameters, establishing a pseudopolymorphic relationship, which is a special case of polymorphism.[39] As described in the literature, polymorphism is a common phenomenon in crystals, in which the solids formed by the same substance crystallize in different arrangements with identical chemical composition, while furthermore, its extended form – pseudopolymorphism – can be also recognized for the solids without a totally identical chemical

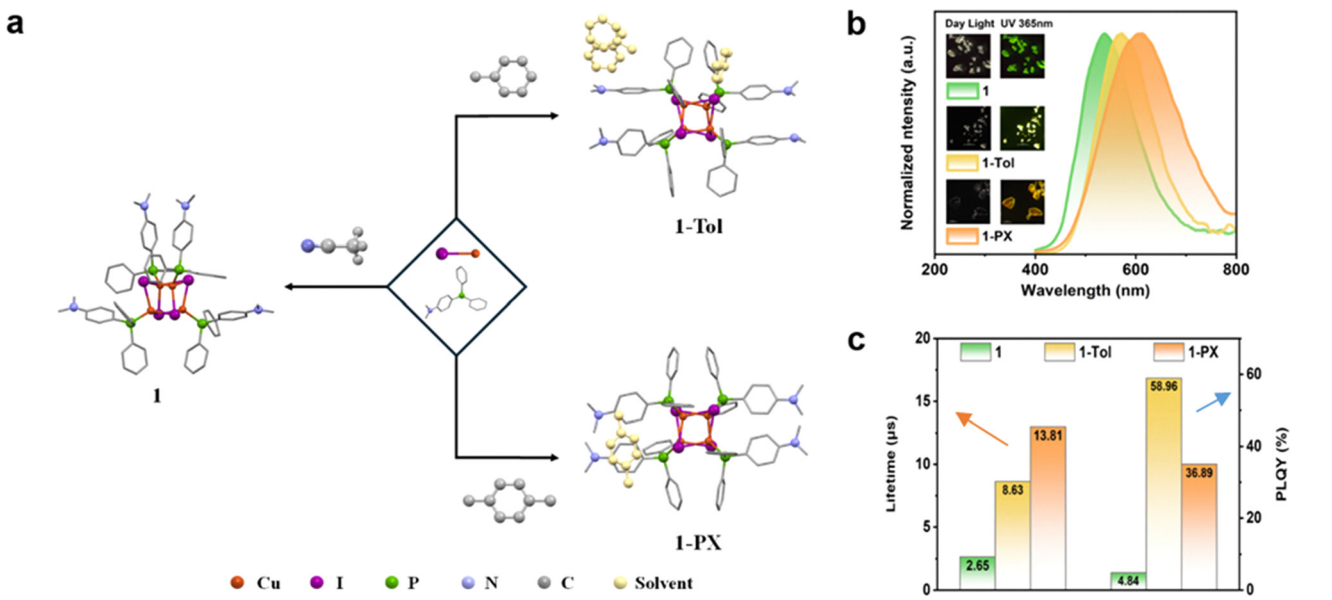

Fig. 1 Structures and photophysical properties of **1**, **1-Tol**, and **1-PX** at room temperature. (a) Schematic diagram of crystal engineering strategy synthesis and single crystal structure diagram of polycrystalline copper(I) iodide clusters, H is omitted for clarity. (b) The normalized emission spectra, insets are the crystal photographs under daylight and 365 nm UV. (c) Lifetime and PLQY.

composition, especially those formed with the same substance yet different solvent molecules during crystallization. In contrast, **1-PX** crystallizes in the space group *C*2/*c*, exhibiting a markedly altered crystal packing arrangement (Fig. S2), confirming that it is a polymorph of **1** and **1-Tol**. Therefore, the three compounds can be related *via* pseudo-polymorphism although they have different solvent environments in the crystal lattice.

Analysis of the data in Tables S4–S6 shows that the coordination bond lengths of **1**, **1-Tol**, and **1-PX** are very similar. The average Cu-P bond lengths are 2.250, 2.258, and 2.254 Å, respectively, while the average Cu–I bond lengths are 2.671, 2.690, and 2.690 Å. However, the Cu–Cu distances within the clusters exhibit significant differences, measuring 2.985 Å, 2.938 Å, and 3.086 Å, respectively. Beyond the variations in the Cu_4I_4 core, the arrangement of the ligands also differs under the regulation of crystal engineering. Using the dimethyl groups of the phosphine ligand as a comparison criterion (Fig. 1a), the unit cell of **1** contains no solvent molecules, resulting in the most unconstrained coordination environment. The four dimethyl groups adopt diverse spatial orientations, resembling upward "antennae" and laterally pointing "double arms." In contrast, the unit cells of **1-Tol** and **1-PX** contain three toluene solvent molecules and one *p*-xylene solvent molecule, respectively, leading to a more uniform spatial arrangement of the four dimethyl groups, resembling laterally pointing "four arms." These results demonstrate that crystal engineering can achieve diverse crystal structures for isomorphous clusters, showcasing a rich diversity in Cu–Cu interactions and crystal packing arrangements. Thermogravimetric analysis (Fig. S3) further verifies the stability of these clusters. The first weight loss step corresponds to the removal of toluene and *p*-xylene, with weight losses matching theoretical values. Additionally, all three clusters begin to decompose at approximately 330 °C, indicating their excellent thermal stability.

To gain deeper insights into the photophysical properties of polymorphic Cu_4I_4(4-dpda)$_4$, we first performed UV-Vis absorption spectroscopy on the solid-state samples. The results showed that their absorption spectra are similar. As shown in Fig. S4a, the main absorption bands were located in the range of 250–400 nm, which can be attributed to π–π* transitions of the benzene ring, n–π* transitions of unsaturated groups, and energy transitions of the metal cluster core.[40] Subsequently, we further investigated their photoluminescence properties at room temperature. The excitation spectrum of **1-Tol** was similar to that of **1**, exhibiting a broad peak in the range of 250–400 nm, while the excitation spectrum of **1-PX** displayed a narrower peak, primarily concentrated in the 300–380 nm range (Fig. S4b). This might be related to its different crystal engineering structure as compared to **1** and **1-Tol**, in which the packing in **1-PX** favours the energy transitions from the metal cluster cores. As shown in Fig. 1b, the emission peaks of **1**, **1-Tol**, and **1-PX** were located at 540, 570, and 605 nm, respectively, corresponding to green, yellow, and orange luminescence. Analysis of the time-resolved decay curves (Fig. S5) revealed that the luminescence lifetimes of all three samples were in the microsecond (μs) range, indicating that their emissions originated from triplet excited states and are characteristic of phosphorescence. As shown in Fig. 1c, the luminescence lifetimes of **1**, **1-Tol**, and **1-PX** were 2.65 μs, 8.63 μs, and 13.81 μs, respectively, with PLQY of 4.84%, 58.96%, and 36.89%. The significantly extended luminescence lifetimes and substantially enhanced PLQY of **1-Tol** and **1-PX** clearly demonstrate the remarkable effectiveness of crystal engineering in enhancing the RTP performance of copper(I) iodide clusters. These results highlight the critical

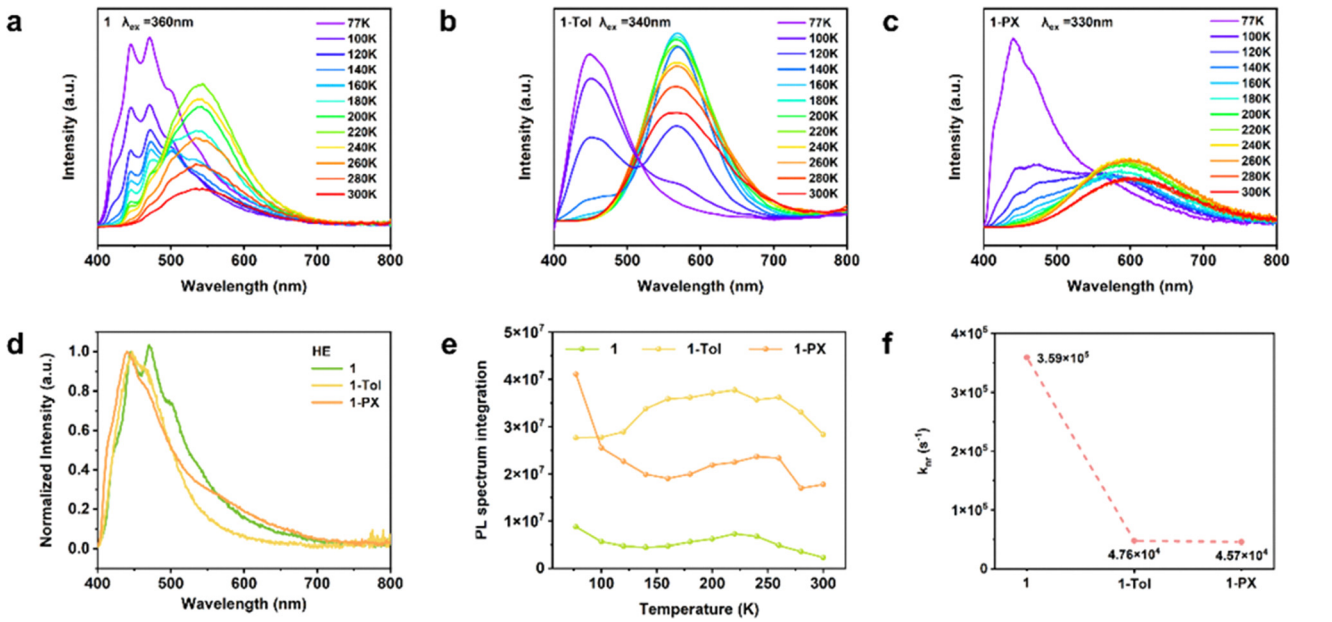

Fig. 2 Research studies on the luminescence properties of **1**, **1-Tol**, and **1-PX**. Temperature-dependent emission spectra of **1** (a), **1-Tol** (b), **1-PX** (c). (d) The emission spectra at 77 K. (e) The integration value of PL spectrum with changing temperature. (f) k_{nr} values at room temperature.

role of crystal engineering in modulating the photophysical properties of materials.

To elucidate the RTP mechanism of polymorphic Cu_4I_4(4-dpda)$_4$, temperature-dependent photoluminescence (PL) measurements were conducted (Fig. 2a–c). Upon cooling from 300 K to 77 K, the original room-temperature emission bands initially intensified before gradually diminishing and eventually disappearing. Concurrently, a new emission band emerged at ~450 nm, characteristic of the dual-emission feature observed in copper(I) iodide clusters, where the room-temperature and low-temperature emissions correspond to the low energy (LE) and high energy (HE) bands, respectively. The temperature-dependent PL spectra of ligand 4-dpda (Fig. S6) show a stable blue emission peak at ~450 nm, with intensity decreasing monotonically as temperature rises. This distinct thermal response differs sharply from that of copper(I) iodide clusters, excluding ligand-centered phosphorescence mechanisms. Together with the LE emission characteristics of the clusters, the observed RTP is attributed to the ^{3}CC excited state.

Although **1** and **1-Tol** crystallize in the same space group of the triclinic system with similar packing arrangements, the PLQY of **1-Tol** is significantly enhanced, reaching 12 times that of **1**. The room-temperature emission of the copper(I) iodide cluster is closely related to energy transfer within the cluster center, which is influenced by cuprophilic interactions. In **1-Tol**, the shorter Cu–Cu distance enhances this interaction, stabilizing the energy transition and lowering the energy level of the LE emissive state,[41] thereby causing its emission peak to red-shift from 540 nm (as in **1**) to 570 nm. Additionally, the crystal packing enhances lattice rigidity, suppressing non-radiative triplet exciton transitions at room temperature, thereby significantly improving RTP.

To verify the mechanism of crystal engineering effect in **1-Tol**, we heated **1-Tol** powder in a vacuum oven at 120 °C for 5 days to remove the toluene solvent, obtaining the desolvated sample **1-Tol-hong**. High-resolution XPS results (Fig. S8) showed that Cu remained in the monovalent state. The PXRD pattern (Fig. S9a) revealed broader and fewer diffraction peaks, indicating transformed crystal packing. TG analysis (Fig. S9b) confirmed removal of the solvent. As shown in Fig. S10, under 365 nm UV excitation, **1-Tol-hong** emitted yellow-green light with a 15 nm blue-shifted emission peak and PLQY reduced to 8.60% compared with **1-Tol**. This indicates that the removal of toluene not only decreased the compactness of the Cu_4I_4 core, leading to an elevated LE emissive state energy level and blue-shifted emission, but also significantly weakened crystal rigidity, resulting in a marked reduction in RTP efficiency. Subsequently, we conducted a series of photoluminescence tests on **1-Tol-hong** under variable-temperature conditions (Fig. S11 and S12). Comparative analysis revealed that the luminescence properties of **1-Tol-hong** changed significantly, becoming more similar to those of **1**. Owing to the similar solid-state chemical environments of different copper(I) iodide clusters, their excited-state distortion levels show consistency in the LE band. Among the polymorphic copper(I) iodide clusters, **1-PX** exhibits the largest Cu–Cu distance but the lowest LE energy level. Due to significant structural differences between **1-PX** and the other two copper(I) iodide clusters, the degree of excited-state distortion varies, making it hard to directly compare the strength of cuprophilic interactions based solely on Cu–Cu distances, while the substantial enhancement of RTP in **1-PX** is a direct outcome of the crystal engineering effect. These findings highlight the dual role of crystal engineering: it not only modulates the self-assembly process to significantly enhance cuprophilic interactions but also actively participates in the crystallization process, markedly improving crystal rigidity and effectively reducing non-radiative transitions, thereby greatly enhancing RTP efficiency.

To gain deeper insights into the mechanism of RTP enhancement, the temperature-dependent luminescence properties of the three samples were systematically investigated. As shown in Fig. 2d, the HE positions are similar, all located near 450 nm in the blue region, and align well with the PL spectrum of 4-dpda (Fig. S6), suggesting that HE can be attributed to XLCT or MLCT. Furthermore, analysis of the luminescence decay curves reveals millisecond-scale lifetimes for both **1-Tol** and **1-PX** at low temperatures (Fig. S7), confirming that their HE originates from ^{3}X/MLCT.

An isosbestic point was observed in the overlapping region of the two energy bands (HE and LE) of **1**, **1-Tol**, and **1-PX**. Using this point as the boundary, the emission spectra on both sides were integrated, and the activation energy data were calculated using the Arrhenius equation.[42] As shown in Fig. S13, the calculated activation energies for **1**, **1-Tol**, and **1-PX** are 600, 859, and 410 J, respectively. The lower activation energy barriers of **1-PX** and **1** suggest that the transition from HE to LE is more favorable. However, complete quenching of the HE emission band occurs only above 220 K for **1-PX** and 290 K for **1**, whereas the HE emission band of **1-Tol** is fully quenched above 160 K. Analysis of the lifetime measurements reveals that the HE lifetime of **1-Tol** decreases with increasing temperature, consistent with typical phosphorescence behavior. In contrast, the HE emission states of **1** and **1-PX** exhibit an increase in lifetime with rising temperature within the range of 77–140 K. Based on these findings, we propose that the relatively low energy barriers in **1** and **1-PX** result in partial excitons re-transitioning back to the HE level during the energy transfer process from HE to LE. These re-transitioned excitons subsequently decay radiatively to the ground state, leading to an extended HE lifetime and a slower quenching of the HE emission state. Furthermore, the incomplete energy transfer results in a relatively modest increase in the intensity of the LE band.

To investigate the dynamic evolution of PLQY with temperature, we integrated the emission spectra of **1**, **1-Tol**, and **1-PX** in the wavelength range of 400–800 nm, based on the positive correlation between spectral integral area and PLQY, yielding the results shown in Fig. 2e. At 77 K, the luminescence intensities follow the order **1-PX** > **1-Tol** > **1**, indicating that structural modifications in the copper(I) iodide clusters significantly affect both LE and HE emissions. The integral value of **1-Tol** increases continuously from 77 to 220 K, suggesting

efficient energy transfer from HE excitons to the LE emission band. Consequently, at 300 K, **1-Tol** achieves the highest PLQY (58.96%), which is 12 times that of **1**. In contrast, for **1-PX**, incomplete energy transfer leads to a weaker enhancement of LE emission compared to the reduction in HE emission. As a result, its integral value decreases gradually from 77 to 160 K and only begins to recover slowly above 160 K. Thus, at 300 K, **1-PX** exhibits a relatively lower PLQY of 36.89%. However, due to its stronger LE emission (approximately four times that of **1**), its PLQY still shows significant improvement compared to **1**.

Subsequently, the non-radiative decay rate (k_{nr}) at room temperature was calculated using following equation:[26]

$$k_{nr} = \frac{1 - \Phi}{\bar{\tau}} \quad (1)$$

where Φ is the PLQY, $\bar{\tau}$ is the average photoluminescence lifetime. As shown in Fig. 2f, the k_{nr} values of **1-Tol** and **1-PX** are one order of magnitude lower than that of **1**, demonstrating that the crystal engineering strategy effectively suppresses TQ of the copper(I) iodide clusters, thereby enhancing RTP.

Theoretical calculations were conducted for **1**, **1-Tol**, and **1-PX** using density functional theory (DFT). The spatial distributions of the highest occupied molecular orbital (HOMO) and the lowest unoccupied molecular orbital (LUMO) were visualized using Multiwfn[43] in combination with the VMD program. As illustrated in Fig. 3a, the HOMO of the three polymorphic Cu_4I_4(4-dpda)$_4$ clusters is predominantly localized on the Cu_4I_4 core, while the LUMO is distributed over the aromatic rings of the ligands. The energy gap between the HOMO and LUMO aligns with the trend observed in the experimentally determined excitation energies (**1-PX** > **1-Tol** > **1**). Notably, the LUMO of **1** and **1-Tol** is primarily concentrated on a single ligand, whereas for **1-PX**, it is distributed across two ligands. This results in a significant enhancement in charge transfer efficiency for **1-PX**, leading to the strongest HE emission. These findings underscore the profound impact of crystal packing modes on the distribution of molecular orbitals and energy level transitions.

Based on the synergistic analysis of experimental and theoretical calculations, the luminescence mechanism illustrated in Fig. 3b was proposed. For the three compounds, the emission at low temperature is dominated by the HE state. However, along with the temperature rise, the HE excitons begin energy transition to populate the LE emission. The crystal packing in the compounds undergoes an alteration in the energy barrier, which further affects energy transition rate and inhibits thermal quenching, thereby achieving balance of the two key processes. For **1-Tol**, the improvement in RTP performance is mainly attributed to the strengthened cuprophilic interactions and enhanced structural rigidity achieved through crystal engineering, which effectively boosts HE emission. Additionally, the appropriate energy barrier design facilitates efficient energy transfer. In contrast, **1-PX** achieves a substantial optimization of charge transition efficiency by modulating the crystal packing mode *via* crystal engineering, leading to a significant enhancement in HE emission. Both factors effectively suppressed thermal quenching, thereby ultimately realizing a significant enhancement in RTP.

Owing to the pronounced spectral variations observed in copper(I) iodide clusters during temperature changes, we investigated their potential application as temperature sensors (Fig. S14–S16). The temperature sensing of **1** and **1-Tol** is divided into dual modes. Taking **1-Tol** as an example, in the low-temperature response region (100–160 K), the logarithmic value of the intensity ratio between its LE and HE emissions shows a linear response to temperature changes. A linear equation with R^2 = 0.99279 was obtained by fitting the scatter plot. In the high-temperature response region (260–380 K), the spectrum exhibits a single LE emission peak. Fitting the intensity of this peak with temperature yields a linear equation with R^2 = 0.99788, indicating that the emission intensity decreases by an average of 0.616% per 1 K. Notably, **1-Tol** demonstrates the highest sensitivity in the low-temperature region, with the logarithmic value showing a linear

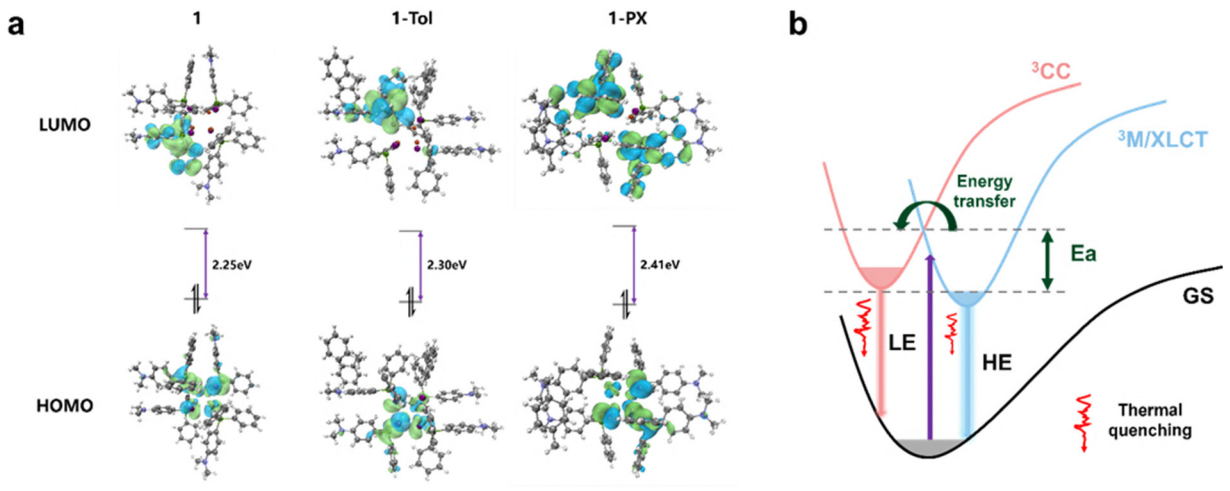

Fig. 3 Theoretical calculation and mechanism. (a) DFT-calculated HOMO and LUMO molecular orbitals of **1**, **1-Tol**, and **1-PX**. (b) Schematic diagram of luminescence mechanism.

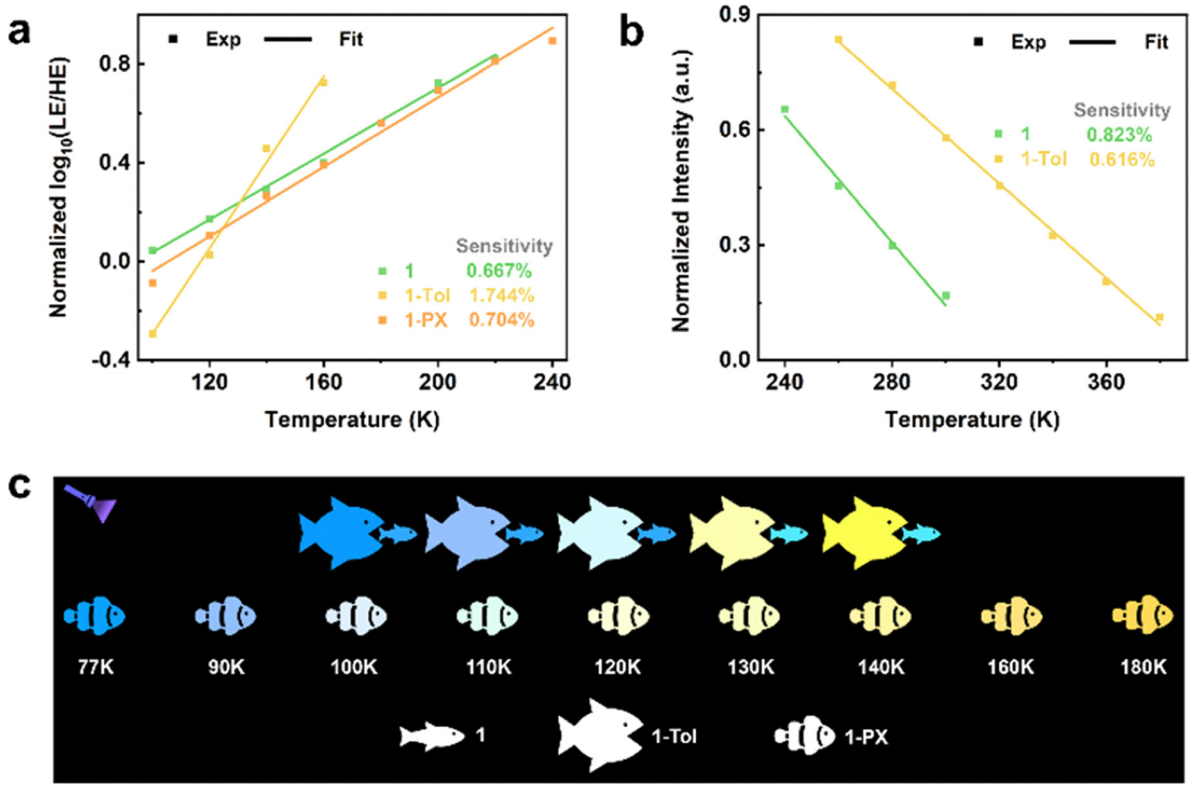

Fig. 4 The applications of $Cu_4I_4(4\text{-dpda})_4$ clusters. (a) Linear correlation between logarithm value of the intensity ratio of LE/HE and temperature **1**, **1-Tol**, and **1-PX**. (b) Linear correlation between LE intensity and temperature of **1** and **1-PX**. (c) Schematic representation of **1**, **1-Tol**, and **1-PX** as temperature pigment.

response that increases by an average of 1.744% per 1 K, approximately 2.6 times that of **1** and 2.5 times that of **1-PX** (Fig. 4a and b). Additionally, **1-PX** and **1-Tol** respectively broaden the temperature response ranges in the low-temperature and high-temperature regions. In particular, **1-Tol** exhibits a high-temperature response range twice that of **1**. These results indicate that crystal engineering significantly alters their thermochromic properties.

Moreover, due to the similar position of the HE emission peak, the redshift of the LE emission peak enhances the thermochromic effect of the copper(I) iodide clusters, making the color differences more pronounced and easily recognizable during temperature changes. As shown in Fig. 4c, within the temperature range of 77 K to 300 K, **1** undergoes a color change from blue to cyan to green, primarily within the cool light region. In contrast, **1-Tol** exhibits a transition from deep blue to sky blue to yellow, completed within the 100–140 K temperature range, making it suitable as a colorimetric thermometer for this interval. **1-PX** displays the widest thermochromic range, covering a color progression from blue to cyan to yellow to orange. This highlights the potential for use as a "temperature pigment" and for multicolor display applications.

Conclusions

In summary, we successfully prepared three polymorphic copper(I) iodide clusters, **1**, **1-Tol** and **1-PX**, manifesting significantly enhanced RTP performance through a crystal engineering strategy. They exhibit notable structural differences, primarily reflected in the strength of cuprophilic interactions and variations in crystal packing modes. By combining single-crystal structure analysis, spectroscopic measurements, and theoretical calculations, we elucidated the distinct HE/LE energy transfer and thermal quenching variations underlying the enhanced RTP in **1-Tol** and **1-PX**. This study highlights the flexibility and adaptability of crystal engineering in tuning material properties, providing an excellent platform for understanding and optimizing RTP performance. Furthermore, leveraging the significantly enhanced thermochromic effect achieved through crystal engineering, we explored the potential applications of **1-Tol** and **1-PX** in temperature sensing and multicolor display. The results demonstrate that the materials exhibit remarkable improvements in RTP sensitivity and response range, laying a solid foundation for their practical use in intelligent optical devices.

Conflicts of interest

There are no conflicts to declare.

Data availability

The data will be available from the authors upon request.

Supplementary information: All experimental and characterisation data, as well as photophysical and NMR spectra. See DOI: https://doi.org/10.1039/d5qm00636h.

CCDC 2169865, 2402247 and 2402248 contain the supplementary crystallographic data for this paper.[44a–c]

Acknowledgements

This work was supported by the NKRD Program of China (2021YFA1500401) and the NSFC (22171291, 92461302, and 92261114).

Notes and references

1 X. F. Luo, B. Tian, Y. X. Zhai, H. D. Guo, S. X. Liu, J. Li, S. J. Li, T. D. James and Z. J. Chen, Room-temperature phosphorescent materials derived from natural resources, *Nat. Rev. Chem.*, 2023, **7**, 800–812.

2 H. Zheng, Z. Y. Zhang, S. Z. Cai, Z. F. An and W. Huang, Enhancing purely organic room temperature phosphorescence *via* supramolecular self-assembly, *Adv. Mater.*, 2024, **36**, 2311922.

3 X. Li, Y. F. Wang, Z. Y. Zhang, S. Z. Cai, Z. F. An and W. Huang, Recent advances in room-temperature phosphorescence metal-organic hybrids: structures, properties, and applications, *Adv. Mater.*, 2024, **36**, 2308290.

4 J.-X. Wang, L. Gutiérrez-Arzaluz, X. Wang, T. He, Y. Zhang, M. Eddaoudi, O. M. Bakr and O. F. Mohammed, Heavy-atom engineering of thermally activated delayed fluorophores for high-performance X-ray imaging scintillators, *Nat. Photonics*, 2022, **16**, 869–875.

5 Q.-S. Zhang, X.-D. Zhang, J.-Y. Zhuang and M. Pan, Highly two-photon and X-ray excited long-persistent luminescence in a crystalline host-guest aggregate, *Aggregate*, 2024, **5**, e456.

6 Y. X. Lei, W. B. Dai, G. C. Li, Y. F. Zhang, X. B. Huang, Z. X. Cai and Y. P. Dong, Stimulus-responsive organic phosphorescence materials based on small molecular host-guest doped systems, *J. Phys. Chem. Lett.*, 2023, **14**, 1794–1807.

7 Y. H. Zhang, H. R. Li, M. D. Yang, W. B. Dai, J. B. Shi, B. Tong, Z. X. Cai, Z. Y. Wang, Y. P. Dong and X. Q. Yu, Organic room-temperature phosphorescence materials for bioimaging, *Chem. Commun.*, 2023, **59**, 5329–5342.

8 X. Xu and B. Yan, Recent advances in room temperature phosphorescence materials: design strategies, internal mechanisms and intelligent optical applications, *Phys. Chem. Chem. Phys.*, 2023, **25**, 1457–1475.

9 Y. J. Li and P. F. Gao, Emerging luminescent materials for information encryption and anti-counterfeiting: stimulus-response aiegens and room-temperature phosphorescent materials, *Chemosensors*, 2023, **11**, 489.

10 X. Y. Dou, X. Wang, X. L. Xie, J. Zhang, Y. Li and B. Tang, Advances in polymer-based organic room-temperature phosphorescence materials, *Adv. Funct. Mater.*, 2024, **34**, 2314069.

11 T. T. Li, N. Zhang, S. Zhao, M. Z. Liu, K. Zhang, C. Zhang, J. Shu and T.-F. Yi, Long-lived dynamic room temperature phosphorescent carbon dots for advanced sensing and bioimaging applications, *Coord. Chem. Rev.*, 2024, **516**, 215987.

12 J. Troyano, F. Zamora and S. Delgado, Copper(I)-iodide cluster structures as functional and processable platform materials, *Chem. Soc. Rev.*, 2021, **50**, 4606–4628.

13 W. Liu, Y. Fang and J. Li, Copper iodide based hybrid phosphors for energy-efffcient general lighting technologies, *Adv. Funct. Mater.*, 2018, **28**, 1705593.

14 O. Caballero-Calero, J. R. Ares and M. Martín-González, Environmentally friendly thermoelectric materials: high performance from inorganic components with low toxicity and abundance in the earth, *Adv. Sustainable Syst.*, 2021, **5**, 2100095.

15 M.-H. Fang, Z. Bao, W.-T. Huang and R.-S. Liu, Evolutionary generation of phosphor materials and their progress in future applications for light-emitting diodes, *Chem. Rev.*, 2022, **122**, 11474–11513.

16 X.-L. Ding, L. Shen, L.-Y. Zou, M.-S. Ma and A.-M. Ren, A theoretical investigation on the neutral Cu(I) phosphorescent complexes with azole-based and phosphine mixed ligand, *Mol. Phys.*, 2018, **116**, 898–909.

17 A. Kobayashi and M. Kato, Stimuli-responsive luminescent copper(I) complexes for intelligent emissive devices, *Chem. Lett.*, 2017, **46**, 154–162.

18 Z. Wang, J.-J. Liu, S.-Y. Yin, M.-Y. Li, Y.-J. Hou, D. Wang, J.-T. Mo and G. Chen, Ultralong near infrared room temperature phosphorescence in Cu(I) metal-organic framework based-on D–π–A–π–D linkers, *Adv. Funct. Mater.*, 2023, **33**, 2212985.

19 Q. S. Hu, C. K. Zhang, X. Wu, G. J. Liang, L. Wang, X. W. Niu, Z. Wang, W.-D. Si, Y. B. Han, R. Q. Huang, J. W. Xiao and D. Sun, Highly effective hybrid copper(I) iodide cluster emitter with negative thermal quenched phosphorescence for X-ray imaging, *Angew. Chem., Int. Ed.*, 2023, **62**, e202217784.

20 H. X. Miao, X. C. Pan, M. Li, W. J. Zhaxi, J. Wu, Z. T. Huang, L. Y. Liu, X. Ma, S. L. Jiang, W. Huang, Q. Zhang and D. Y. Wu, A copper iodide cluster-based coordination polymer as an unconventional zero-thermal-quenching phosphor, *Inorg. Chem.*, 2022, **61**, 18779–18788.

21 J. Ohshita, T. Kai, Y. Adachi, K. Yamaji, M. Nakamura, S. Watase, S. Mori and N. Matsuyama, Synthesis of nonplanar bipyridyls bridged by disilane and disiloxane and their phosphorescent copper complexes, *Appl. Organometal. Chem.*, 2020, **34**, e5306.

22 X. Q. Ji, Y. Liu, R. Q. Li, Z. X. Zhang, X. Y. Zhang, C. C. Chen, J. Chen, H. P. Lu, R. Chen and L. L. Mao, Mono- and bidentate chiral ligands lead to efficient circularly polarized luminescence in 0D and 3D semiconducting copper(I) iodides, *Adv. Opt. Mater.*, 2023, **11**, 2300541.

23 W.-T. Chen, L. Chen, Z.-Y. Liang, Z.-W. Mo, J.-W. Ye and X.-M. Chen, Multiple flexibilities trigger luminescent

piezochromism of closely packed Cu(I) coordination polymers, *Adv. Opt. Mater.*, 2023, **11**, 2202771.

24 J. Chatterjee, R. Tanwar, A. Chatterjee, M. D. Ambhore, M. Kabir, P. Mandal and P. Hazra, Controlling triplet-harvesting pathways and nonlinear optical properties in Cu(I) iodide-based polymers through ligand engineering, *J. Phys. Chem. Lett.*, 2025, **16**, 1549–1558.

25 C. Chen, R.-H. Li, B.-S. Zhu, K.-H. Wang, J.-S. Yao, Y.-C. Yin, M.-M. Yao, H.-B. Yao and S.-H. Yu, Highly luminescent inks: aggregation-induced emission of copper-iodine hybrid clusters, *Angew. Chem., Int. Ed.*, 2018, **57**, 7106–7110.

26 Y.-E. Shi, J. Z. Ma, A. R. Feng, Z. G. Wang and A. L. Rogach, Aggregation-induced emission of copper nanoclusters, *Aggregate.*, 2021, **2**, e112.

27 M. X. Yang, X.-L. Chen and C.-Z. Lu, Efficiently luminescent copper(I) iodide complexes with crystallization-induced emission enhancement (CIEE), *Dalton Trans.*, 2019, **48**, 10790–10794.

28 L. Chen, X.-B. Dong, H.-Y. Liao, W.-J. Zhang, Z.-W. Mo, H.-P. Wang, J.-W. Ye and X.-M. Chen, Long-range rigidity induced ultralong cluster-centered phosphorescence, *Chem. Mater.*, 2022, **34**, 9182–9189.

29 L.-Z. Feng, J.-J. Wang, T. Ma, Y.-C. Yin, K.-H. Song, Z.-D. Li, M.-M. Zhou, S. Jin, T. T. Zhuang, F.-J. Fan, M.-Z. Zhu and H.-B. Yao, Biomimetic non-classical crystallization drives hierarchical structuring of efficient circularly polarized phosphors, *Nat. Commun.*, 2022, **13**, 3339.

30 C.-Y. Liu, X.-R. Chen, H.-X. Chen, Z. Niu, H. Hirao, P. Braunstein and J.-P. Lang, Ultrafast luminescent light-up guest detection based on the lock of the host molecular vibration, *J. Am. Chem. Soc.*, 2020, **142**, 6690–6697.

31 W.-J. Zhang, W.-T. Chen, C.-H. Li, W.-Z. Sun, J.-W. Ye, L. Chen, H.-P. Wang and X.-M. Chen, Luminescence detection of CH_2Cl_2 by varying Cu···Cu interactions in a flexible porous coordination polymer, *Inorg. Chem. Front.*, 2023, **10**, 6909–6917.

32 Q. Benito, X. F. Le Goff, S. Maron, A. Fargues, A. Garcia, C. Martineau, F. Taulelle, S. Kahlal, T. Gacoin, J.-P. Boilot and S. Perruchas, Polymorphic copper iodide clusters: insights into the mechanochromic luminescence properties, *J. Am. Chem. Soc.*, 2014, **136**, 11311–11320.

33 R. An, Q. S. Wang, Y. Liang, P. Y. Du, P. P. Lei, H. Z. Sun, X. Y. Wang, J. Feng, S. Y. Song and H. J. Zhang, Reversible structural phase transitions in zero-dimensional Cu(I)-based metal halides for dynamically tunable emissions, *Angew. Chem., Int. Ed.*, 2024, **64**, e202413991.

34 J. Chen, S. N. Geng, X. Y. Zhang, X. Pan, C. C. Chen, R. Q. Li, J. Q. Wen, C. Sun, R. Chen, Z. W. Xiao and L. L. Mao, Isomeric zero-dimensional hybrid copper(I) iodides as highly efficient multicolor phosphors, *ACS. Mater. Lett.*, 2024, **6**, 865–876.

35 Q. Benito, I. Maurin, T. Cheisson, G. Nocton, A. Fargues, A. Garcia, C. Martineau, T. Gacoin, J.-P. Boilot and S. Perruchas, Mechanochromic luminescence of copper iodide clusters, *Chem. – Eur. J.*, 2015, **21**, 5892–5897.

36 S. J. Zhou, S. S. Zhang, H. P. Li, D. Sun, J. Z. Zhang and X. Xin, Solvent-induced self-assembly of copper nanoclusters for white light emitting diodes, *ACS Appl. Nano Mater.*, 2021, **4**, 10911–10920.

37 C. K. Zhang, W.-D. Si, Z. Wang, A. Dinesh, Z.-Y. Gao, C.-H. Tung and D. Sun, Solvent-mediated hetero/homo-phase crystallization of copper nanoclusters and superatomic kernel-related NIR phosphorescence, *J. Am. Chem. Soc.*, 2024, **146**, 10767–10775.

38 X.-C. Shan, F.-L. Jiang, L. Chen, M.-Y. Wu, J. Pan, X.-Y. Wan and M.-C. Hong, Using cuprophilicity as a multi-responsive chromophore switching color in response to temperature, mechanical force and solvent vapors, *J. Mater. Chem. C*, 2013, **1**, 4339–4349.

39 X.-D. Tao, W.-X. Chai, L. Song, Q.-H. Wei, H.-S. Shi and L.-S. Qin, Two luminescent pseudo-polymorphic cuprous complexes with different optical properties: synthesis, characterization and TD-DFT calculations, *Polyhedron*, 2018, **144**, 36–43.

40 E. Cariati, E. Lucenti, C. Botta, U. Giovanella, D. Marinotto and S. Righetto, Cu(I) hybrid inorganic-organic materials with intriguing stimuli responsive and optoelectronic properties, *Coord. Chem. Rev.*, 2016, **306**, 566–614.

41 S. Perruchas, C. Tard, X. F. L. Goff, A. Fargues, A. Garcia, S. Kahlal, J.-Y. Saillard, T. Gacoin and J.-P. Boilot, Thermochromic luminescence of copper iodide clusters: the case of phosphine ligands, *Inorg. Chem.*, 2011, **50**, 10682–10692.

42 C. Tard, S. Perruchas, S. Maron, X. Goff, F. Guillen, A. Garcia, J. Vigneron, A. Etcheberry, T. Gacoin and J. Boilot, Thermochromic luminescence of Sol−Gel films based on copper iodide clusters, *Chem. Mater.*, 2008, **20**, 7010–7016.

43 T. Lu and F. W. Chen, Multiwfn: a multifunctional wavefunction analyzer, *J. Comput. Chem.*, 2012, **33**, 580–592.

44 (*a*) Y.-T. Huang, W. He, J.-Z. Dong, Y.-N. Fan, Z.-W. Wei and M. Pan, CCDC 2169865: Experimental Crystal Structure Determination, 2025, DOI: **10.5517/ccdc.csd.cc2btxnr**; (*b*) Y.-T. Huang, W. He, J.-Z. Dong, Y.-N. Fan, Z.-W. Wei and M. Pan, CCDC 2402247: Experimental Crystal Structure Determination, 2025, DOI: **10.5517/ccdc.csd.cc2lmqvt**; (*c*) Y.-T. Huang, W. He, J.-Z. Dong, Y.-N. Fan, Z.-W. Wei and M. Pan, CCDC 2402248: Experimental Crystal Structure Determination, 2025, DOI: **10.5517/ccdc.csd.cc2lmqwv**.